ACS APPLIED MATERIALS & INTERFACES

www.acsami.org

Research Article

Premelting-Induced Agglomeration of Hydrates: Theoretical Analysis and Modeling

Ngoc N. Nguyen,* Rüdiger Berger, and Hans-Jürgen Butt*

Cite This: *ACS Appl. Mater. Interfaces* 2020, 12, 14599–14606

Read Online

ACCESS | Metrics & More | Article Recommendations | Supporting Information

ABSTRACT: Resolving the long-standing problem of hydrate plugging in oil and gas pipelines has driven an intense quest for mechanisms behind the plug formation. However, existing theories of hydrate agglomeration have critical shortcomings, for example, they cannot describe nanometer-range capillary forces at hydrate surfaces that were recently observed by experiments. Here, we present a new model for hydrate agglomeration which includes premelting of hydrate surfaces. We treat the premelting layer on hydrate surfaces such as a thin liquid film on a substrate and propose a soft-sphere model of hydrate interactions. The new model describes the premelting-induced capillary force between a hydrate surface and a pipe wall or another hydrate. The calculated adhesive force between a hydrate sphere (R = 300 μm) and a solid surface varies from 0.3 mN on a hydrophilic surface (contact angle, θ = 0°) to 0.008 mN on a superhydrophobic surface (θ = 160°). The initial contact area is 4 orders of magnitude smaller than the cross-sectional area of the hydrate sphere and can expand with increasing contact time because of the consolidation of hydrate particles on the solid surface. Our model agrees with the available experimental results and can serve as a conceptual guidance for developing a chemical-free environmentally friendly method for prevention of hydrate plugs via surface coating of pipe surfaces.

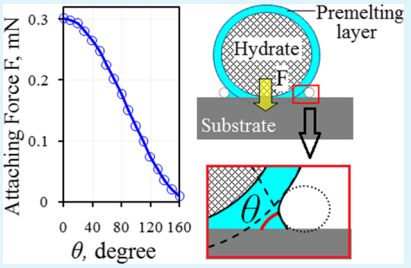

KEYWORDS: *hydrate agglomeration, capillary force, hydrate plug, flow blockage, surface premelting, hydrate formation, blockage modeling*

1. INTRODUCTION

Pipelines are used for transporting crude oils and natural gases from drilling sites to processing complexes. Crude oils contain certain fractions of water in the form of emulsified water droplets such as water-in-oil emulsions. Water may come from different sources. Water can exist together with oils in geological pore structures and is extracted out from the pores concurrently with oils.[1] Water may also be injected into the wells during extraction of oils to compensate the pressure drop in the wells. After multiple-stage separation at drilling sites, the mass fraction of water in crude oils is reduced to below 1% (ref 1), which is also the fraction of water in crude oils in pipelines. Experiments indicated that the diameters of emulsified water droplets in crude oils are typically in the range between 1 and 300 μm.[2]

The presence of emulsified water in crude oils results in a long-standing issue because it tends to block the flow by hydrate formation.[3,4] Typical conditions under deep seas are hydrostatic pressures of hundreds of bars and temperatures of a few degree celsius.[5] These conditions favor the crystallization of gas-saturated emulsified water droplets to form hydrate particles.[6,7] The hydrate particles are ice-like solids composed of water and hydrocarbon gases in which gas molecules are incorporated into hydrogen-bonded structures formed by water molecules.[7−11] The sizes of the resulting hydrate particles are comparable with those of initial water droplets.

Suspended hydrate particles can be harmless since they can be safely transported with the flow. However, turbulent conditions in pipelines can bring the hydrate particles into contact with the pipe wall (Figure 1a). Even so, the attached hydrate particles may detach again because of viscous shear forces or slide on the pipe wall (Figure 1b). At some locations where the pipe surface has defects in topology, the attaching forces might increase and surpass detaching forces (Figure 1c). A similar situation might happen when the pipe surface has inhomogeneous chemistry caused by corrosions, contaminations, or even by soldering processes. When the attaching forces overcome detaching forces, a stable attachment is established (Figure 1c). Once the first hydrate particle has stably attached to the pipe wall, the attaching forces of the following hydrate particles increase owing to synergistic interactions between the particles (Figure 1d). The latter enables a steady hydrate mass growth on the pipe wall (Figure 1e) which ultimately produces a hydrate plug. This conceptual picture leads to a central question: What are the relevant

Received: January 12, 2020
Accepted: March 3, 2020
Published: March 3, 2020

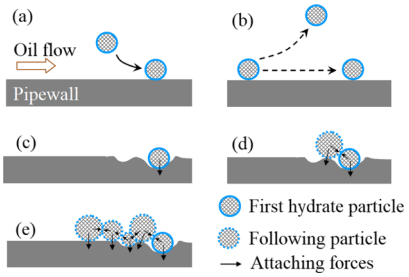

Figure 1. Conceptual depiction of the attachment of hydrate particles to a pipe wall. (a) Turbulences bring hydrate particles in contact with the pipe wall. (b) Attached hydrate particles may detach again because of viscous shear forces or slide on the pipe wall. (c) Stable attachment is only established if the attaching forces overcome detaching forces. The holes on the substrate represent uneven surface topology or inhomogeneous surface chemistry. (d,e) Attachment of the following hydrate particles is favorable because of synergistic interactions between hydrate particles, leading to a steady growth of a hydrate plug. The drawings are not to scale.

attractive forces for hydrate particles versus a pipe wall and other hydrate particles?

Already, a simple photograph of a hydrate plug provides hints about the forces that underpin the formation of a hydrate plug (Figure 2). The hydrate plug has a ring shape, indicating

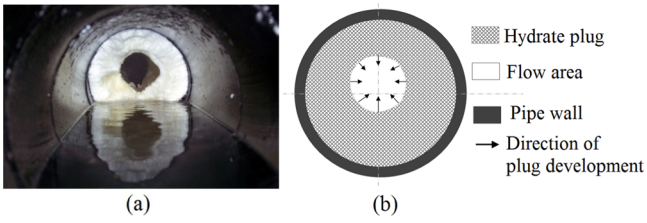

Figure 2. (a) Hydrate plug in the industry (image credited to Offshoreengineering.com). The hydrate plug is a white solid and it reduces the cross-sectional diameter of the pipe by about 70%. Oil flow could transmit only through a narrow channel remaining at the center of the pipe. (b) Profile of a hydrate plug derived from the image on the left side. The ring shape of the hydrate plug implies that gravity is not an important factor.

that hydrate plug formation must initiate evenly at every position on the pipe wall. It grows inward as indicated by arrows (Figure 2b). The hydrate ring is about 30% thicker at the bottom side than at the upper side. This observation of an almost perfect ring-shaped hydrate plug indicates that gravitational sedimentation does not play a dominant role in plug formation. Therefore, forces between hydrate particles and the pipe wall and other hydrate particles play a major role.

Previous studies indicated that capillary forces are important for the agglomeration of hydrate particles. However, the capillary bridges investigated in previous studies were formed by water droplets sitting on top of hydrate particles. In oil flow, these capillary bridges arise from water droplets that have not yet been converted into hydrate particles and are the so-called "free water".[12−16] Then, the capillary force leads to attraction of hydrate particles, linking them together. Thus, suspended hydrate particles might grow in sizes with time as long as "free water" is present in the oil flow. In a similar manner, the unconverted water drops can also form water bridges between hydrate particles and the pipe wall surface. Thus, particles can link to the pipe wall too. Nevertheless, previous works considered hydrate particles as hard spheres. The capillary bridges were formed by water droplets sitting on top of hard hydrate particles. Such a convention led to the argument that capillary forces will disappear when all water droplets in the oil fluid are converted into hydrate particles.[17,18] Oil fluids without water droplets are thought to be "dry" and capillary bridges are believed to vanish because no free water is present any more.[17,18]

However, the recent literature indicates that hydrate surfaces are likely not solid but rather quasi-liquid because of premelting.[19,20] Therefore, classical hard-sphere models can be insufficient for modeling the interactions of hydrates. In particular, a quasi-liquid layer (QLL) was found which alters the interfacial forces of hydrate surfaces.[19] In this case, forces between a silica microsphere and a tetra-butyl ammonium bromide semi-clathrate hydrate surface are essentially dominated by capillary attraction and are much larger than van der Waals (vdW) forces.[19] Hence, the theory of hydrate interactions has to be revisited as capillary attraction cannot be neglected.

This work aims to develop a new model for describing the interfacial interactions between a hydrate particle and a solid surface or between a hydrate particle and a hydrate surface emphasizing the premelting behavior of hydrate surfaces. Our model agrees well with recent experimental observations and it helps to better design new techniques based on surface coatings of pipe surfaces for prevention of hydrate plug formation.

2. MODELING

In our model, for hydrate plug formation, we consider the hydrate surfaces to be premelted. Premelting produces a QLL with a thickness δ on a hydrate surface. We identify several types of processes involved in hydrate plug formation (Figure 3). Suspended hydrate particles can deposit on any locations on the pipe wall regardless of the presence of gravity. Therefore, we define an angular coordinate φ (Figure 3a). Gravitational forces point downward. The interactions between suspended hydrate particles and the pipe wall are responsible for the formation of the first hydrate layer on the pipe surface (Figure 3b). Turbulence can bring a suspended hydrate particle close to the wall. Then, vdW attraction between the particle and pipe wall may become sufficiently strong to let the surface of the QLL get into contact with the wall.[19] The liquid-like film can even deform under the vdW attraction to reach the pipe surface before the hydrate particle actually arrives there.[21−23] As soon as the QLL on the hydrate particle touches the pipe surface, a capillary bridge is formed and pulls the particle further toward the wall, resulting in a contact of the hard bodies (Figure 3).[19] The distance traveled by the hydrate particle under capillary force is of the same order of magnitude as the thickness of the QLL (δ). Once the solid hydrate particle has attached to the pipe wall, the capillary bridge causes an adhesive force to retain the particle on the wall. As a subsequent process during the attachment, the hydrate particle is reshaped, which will be described in Section 2.2. The continuous deposition of the following hydrate particles leads to the formation of a hydrate layer covering the pipe surface.

The hydrate layer can grow in thickness owing to the consecutive deposition of additional hydrate particles. vdW forces attract nearby hydrate particles to the hydrate layer followed by the formation of a capillary bridge (Figure 3c).

https://dx.doi.org/10.1021/acsami.0c00636
ACS Appl. Mater. Interfaces 2020, 12, 14599−14606

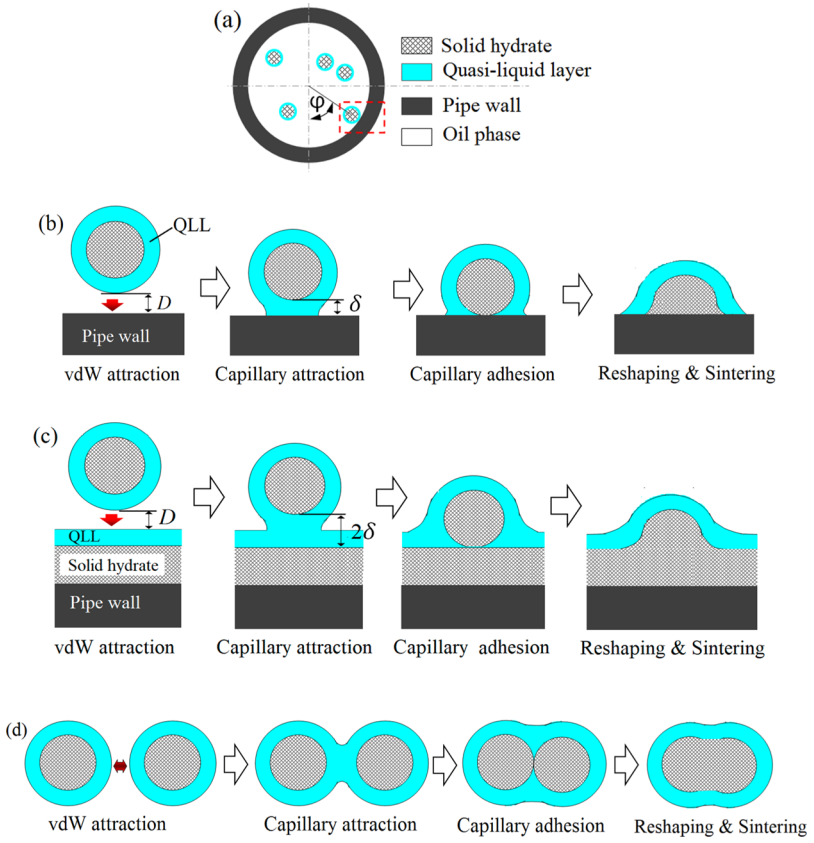

Figure 3. Conceptual scheme of interfacial interactions relevant to the formation of hydrate plugs in pipelines. The hydrate particles are depicted in an ideal spherical shape. The roughness of the pipe wall and the hydrate layer is also neglected for simplicity. The drawings are not to scale.

Capillary forces then drive the hydrate particle further toward the hydrate layer, resulting in a contact of the hard bodies. The distance travelled by the hydrate particle under capillary attraction is in the same order of magnitude of 2δ or twofold QLL thickness. As more hydrate particles attach, the hydrate layer grows in thickness and ultimately forms a plug.

In addition, suspended hydrate particles may aggregate in the oil phase (Figure 3d). If the separation between hydrate particles is in the range of nanometers, vdW forces will become strong enough to aggregate them.[19] The vdW attraction may even lead to deformation of the QLL, enabling particle aggregation over even longer distances.[21−23] As soon as the QLL on each hydrate particle touches the other one, they coalesce to form a capillary bridge that adheres the particles together (Figure 3d). This process leads to an increase in sizes of suspended hydrate particles, which may eventually favor a gravitational sedimentation process.

2.1. vdW and Capillary Force. In the following, we treat the QLL on a hydrate surface similar to a thin liquid film on a solid substrate.[21,22] The interactions between a hydrate particle and a pipe wall comprise vdW interactions prior to the QLL touching the pipe wall and capillary interactions afterward. The vdW force between a hydrate sphere "1" and a pipe wall "2" across oil "3" can be approximated using eq 1, ref 24

$$F_{\mathrm{vdW}} = -\frac{A_{132}R}{6D^2} \tag{1}$$

A negative sign means attractive force. Here, R and D are the radius of the hydrate particle and the particle−pipe wall separation, respectively. A_{132} is the Hamaker constant of the system which can be estimated by

$$A_{132} = (\sqrt{A_{11}} - \sqrt{A_{33}}) \times (\sqrt{A_{22}} - \sqrt{A_{33}}) \tag{2}$$

Here, A_{11}, A_{22}, and A_{33} are Hamaker constants of interactions across vacuum between two identical hydrate surfaces, two identical pipe surfaces, and two identical oil surfaces, respectively.[24,25] Values of A_{ii} are available for a number of materials.[24,25] For example, $A_{22} \cong 4 \times 10^{-19}$ J is a typical value for metals.[25] Metal oxides are typically lower. A_{33} of crude oil can vary depending on the composition of the oil. We use $A_{33} = 0.5 \times 10^{-19}$ J which is a typical value for liquid hydrocarbons.[24] A_{11} of gas hydrates is not available but it can be calculated using eq 3, refs[24,25]

$$A_{11} \cong \frac{3}{4}k_{\mathrm{B}}T\left(\frac{\varepsilon_1 - 1}{\varepsilon_1 + 1}\right)^2 + \frac{3h\nu_{\mathrm{e}}}{16\sqrt{2}}\frac{(n_1^{\,2} - 1)^2}{(n_1^{\,2} + 1)^{3/2}} \tag{3}$$

Here, k_{B}, h, and T are the Boltzmann constant, Planck constant, and the temperature. $\varepsilon_1 \cong 5$ (ref 26) and $n_1 = 1.35$ (ref 27) are the relative permittivity and refractive index of gas hydrates, respectively. $\nu_{\mathrm{e}} = 3 \times 10^{15}$ Hz is the typical absorption frequency.[25] From eq 3, we obtain $A_{11} = 0.77 \times 10^{-19}$ J. Then, from eq 2, we calculate $A_{132} = 0.3 \times 10^{-19}$ J and a vdW force of

$$F_{\mathrm{vdW}} = -5 \times 10^{-21} \times \frac{R}{D^2} \tag{4}$$

Equation 4 expresses the vdW force between a suspended, spherical hydrate particle and a clean pipe wall. This vdW force plays an important role in the initiation of hydrate particle−pipe wall attachment.

https://dx.doi.org/10.1021/acsami.0c00636
ACS Appl. Mater. Interfaces 2020, 12, 14599−14606

When the QLL touches the pipe surface, a three-phase contact and a capillary bridge are formed. From then on, capillary forces dominate.[19] Figure 4 depicts the concepts of

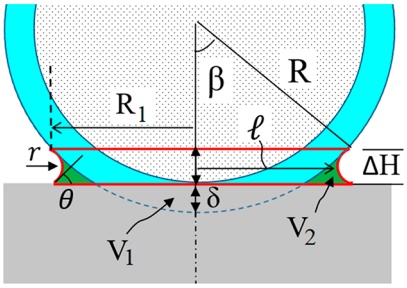

Figure 4. Capillary interaction between a hydrate sphere (dotted) and a pipe wall (gray) in oil (white). The QLL on the hydrate surface is shown in blue. The meniscus that is formed by quasi-liquid squeezed out during the attachment is shown in green. Here, l is the radius of the neck. Other parameters are indicated. The drawings are not to scale.

capillary interactions. When the hydrate sphere attaches to the substrate, the quasi-liquid in the volume V_1 is squeezed out and forms a meniscus which is indicated by green color.

Because the jump into contact is fast, we assume that the total volume of the QLL does not change. Thus, we neglect a possible transition of solid to quasi-liquid or vice versa. Then, the volume (V_2) of the meniscus (highlighted in green) is equal to the volume (V_1) of the quasi-liquid that was squeezed out when the sphere comes to attach to the substrate. Here, the radii of the curvature (l and r) are unknown parameters but they can be calculated based on the geometry of the system (see the Supporting Information)

$$\Delta H = R(1 - \cos\beta) - \delta \tag{5}$$

$$r = [R(1 - \cos\beta) - \delta]/[\cos\beta + \cos\theta] \tag{6}$$

$$R_1 = R \times \sin\beta \tag{7}$$

$$l = R_1 - r(1 - \sin\beta) = R \times \sin\beta - \frac{[R(1 - \cos\beta) - \delta] \times (1 - \sin\beta)}{\cos\beta + \cos\theta} \tag{8}$$

Here, θ is the contact angle of the QLL in oil on the pipe wall surface. The capillary force (F_{ca}) induced by interfacial tension is the integral of the normal component of the surface tension around the neck (F_γ) plus the contribution of the Laplace pressure acting over the contact area ($F_{\Delta P}$), refs[28,29]

$$F_\gamma = -2\pi l\gamma \tag{9}$$

$$F_{\Delta P} = \pi l^2\gamma\left(\frac{1}{l} - \frac{1}{r}\right) \tag{10}$$

$$F_{ca} = -2\pi l\gamma + \pi l^2\gamma\left(\frac{1}{l} - \frac{1}{r}\right) \tag{11}$$

Here, γ is the surface tension of the QLL. To estimate γ, δ, and θ, we assume that interfaces between the QLL and crude oils are analogous to interfaces between water and model oils. This assumption neglects possible effects of natural surfactants in crude oil that might adsorb on the QLL/crude oil interface. We take $\gamma \cong 40$ mN/m that is a typical value for oil−water interfaces. The thickness of the QLL (δ) on gas hydrates is unknown. However, the surface of the semi-clathrate hydrate formed by tetrabutyl ammonium bromide has $\delta \cong 11$ nm at the subcooling $\Delta T = T_e - T = 13°C$[19] where T_e is the equilibrium temperature of bulk melting and T is the working temperature. On ice in air, the thickness of the premelting layer varies from ≅1 nm at $\Delta T \cong 20$ K to 100 nm at ΔT close to 0 °C.[30,31] We use $\delta = 10$ nm as it is a typical thickness of the ice premelting layer at a subcooling of several degree celsius.[30,31] The contact angle θ depends on the wettability of the substrate. Therefore, the remaining unknown parameter is the angle β. However, from $V_1 = V_2$, we can derive an equation for the calculation of β (Supporting Information)

$$R(\sin\beta)^2 \times [R(1 - \cos\beta) - \delta] - [R(1 - \cos\beta)]^2 \times \frac{2 + \cos\beta}{3} - \sin\beta\left[\frac{R(1 - \cos\beta) - \delta}{\cos\beta + \cos\theta}\right]^2 \left(\pi - \theta - \frac{1}{2}\sin 2\theta\right) = 0 \tag{12}$$

We need to solve eq 12 numerically to have β for the given radius R and contact angle θ. Then, we calculate l, F_γ, $F_{\Delta P}$, and F_{ca} using eqs 8−11, respectively. Figure 5a shows, for example,

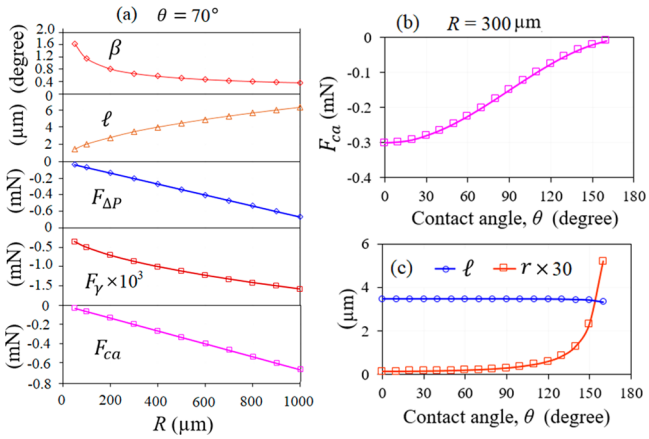

Figure 5. (a) Premelting-induced capillary force for different radii of the hydrate particle for $\theta = 70°$. A negative sign means attractive forces. The angle β was calculated using eq 12. Then, l, F_γ, $F_{\Delta P}$, and F_{ca} were calculated using eqs 8−11, respectively. We used $\delta = 10$ nm and $\gamma = 40$ mN/m. (b) Dependence of capillary force (F_{ca}) on the contact angle θ. The absolute strength of F_{ca} decreases substantially with increasing θ. (c) Small radius of the curvature (r) in the region of small θ is the main reason for strong capillary force. The values of r were scaled by a factor of 30 to better fit the graph.

the results for $\theta = 70°$ which is a typical contact angle of water on pristine stainless steel in oils. The opening angle (β) is small and decreases with increasing particle radius. The reason for small β is that the thickness of the QLL is 5 orders of magnitude smaller compared to the radius of the hydrate particle. The radius of the neck (l) increases from 1.4 to 6.3 μm when R (radius of the hydrate particle) increases from 50 to 1000 μm, which means that the contact area ($A_l = \pi l^2$) is 4 orders of magnitude smaller than the cross-sectional area of the hydrate sphere ($A_R = \pi R^2$). $F_{\Delta P}$ is 3 orders of magnitude greater than F_γ. Hence, we conclude that Laplace pressure-

https://dx.doi.org/10.1021/acsami.0c00636
ACS Appl. Mater. Interfaces 2020, 12, 14599−14606

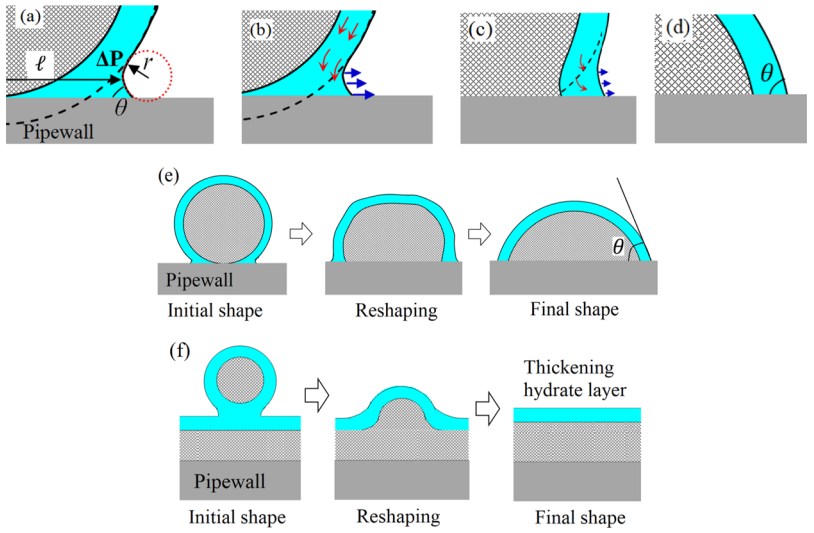

Figure 6. Proposed concepts about three-phase contact line expansion (a–d) and reshaping process (e) for a hydrate sphere attached to a hydrophilic substrate. (f) Reshaping of a hydrate sphere attached to a pre-existing hydrate layer on the pipe wall. The drawings are not to scale.

induced force ($F_{\Delta P}$) is a dominant contribution to capillary force (F_{ca}) between a hydrate particle and a substrate.

To understand the influence of surface hydrophobicity on the capillary force, we calculated F_{ca} as a function of contact angle θ. Figure 5b shows the results for a hydrate particle having R = 300 μm. When the contact angle (θ) increases from 0 to 160°, which means the surface of the substrate changes from hydrophilic to superhydrophobic, the strength of capillary force (F_{ca}) declines from 0.3 mN to 0.008 mN, equivalent to reduction by orders of magnitude. Meanwhile, Figure 5c indicates that the radius of the curvature (r) increases dramatically as the contact angle increases. In contrast to r, the other radius of the curvature (l) decreases slightly from 3.5 μm at θ = 0 to 3.2 μm at θ = 160°. Therefore, based on eq 11, we conclude that the increase in strength of capillary force (F_{ca}) arises from the decrease in the radius of the curvature (r) on a hydrophilic surface.

We have indicated in Figure 1 that an attached hydrate particle will detach again if the detaching forces surpass the attaching forces. Detaching forces are viscous shear forces and their strengths depend upon the turbulent conditions in oil flows. Attaching forces are mainly capillary forces between the hydrate particle and the pipe surface. On a superhydrophobic surface, where capillary forces are reduced by 2 orders of magnitude (Figure 5b) in comparison with those on a hydrophilic surface, attaching forces would no longer exceed detaching forces. As a result, no hydrate particles could attach stably to the pipe surface. Our calculated results in Figure 5 are in good agreement with previous experimental observations on the reduction of hydrate adhesion on hydrophobized surfaces in comparison with hydrophilic surfaces.[32−34]

2.2. Reshaping of Attached Hydrate Particles. After the first attachment, a neck is expected to form near the three-phase contact line (Figure 6a). The curvature induces a Laplace or capillary pressure, ΔP, inside the neck

$$\Delta P = \gamma\left(\frac{1}{l} - \frac{1}{r}\right) \tag{13}$$

The value of ΔP in the meniscus depends on the radii of the curvature (r and l), following eq 13, refs.[28,29] For particles considered here (R > 50 μm), directly after jumping into contact, $l \gg r$. Now, we expect that the pressure deficiency drives the flow of quasi-liquid toward the neck, following red arrows in Figure 6b. For low contact angles of the QLL on the pipe wall, the three-phase contact line expands (the wetting of the surface), following blue arrows. Quasi-liquid flow causes a depletion of the QLL on top of the hydrate particle. Because the thickness of the QLL is constant at a given temperature, depletion of the QLL stimulates the continuous premelting of the hydrate in the upper side, whereas new hydrate is expected to form at the neck because of the arrival of quasi-liquid (Figure 6c). This concept of additional hydrate formation at the neck is similar to the "sintering" effect introduced by Aman et al.[12] However, the underlying physics is different in our case from the "sintering" effect discussed by Aman et al. In our case, the movement of quasi-liquid and formation of additional hydrates at the neck are governed by the thermodynamics of premelting. No new supply of fresh water is involved. In contrast, the "sintering" effect discussed by Aman et al. was ascribed to the apparent growth of hydrates because of new supply of fresh water.[12] The movements of the contact line and of quasi-liquid diminish when a final and thermodynamically stable shape of the hydrate particle is constructed. This final shape is given by the contact angle of the QLL on the pipe wall (Figure 6d). Therefore, the changes in the shape of a hydrate particle after attaching to a pipe wall can follow the one which is proposed in Figure 6e. In the case that a hydrate particle attaches to a pre-existing hydrate layer (Figure 3c), the attached hydrate particle would be ultimately included into the hydrate layer (Figure 6f). As a result, the thickness of the hydrate layer on the pipe wall grows because of continuous deposition of suspended hydrate particles.

Eventually, every freely suspended hydrate particle tends to transform into a thermodynamically stable sphere. The reason is that the curvatures induce a relatively positive Laplace pressure ($+\Delta P_1$) in the QLL at a peak and a relatively negative Laplace pressure ($-\Delta P_2$) in the QLL at a valley on a hydrate surface (Figure 7). The resulting pressure gradient drives a quasi-liquid flow from the peak to the valley. As the thickness of the QLL is constant at a given temperature, the removal of quasi-liquid from the peak stimulates the premelting of the hydrate and erodes the peak. In contrast, new hydrate would

https://dx.doi.org/10.1021/acsami.0c00636
ACS Appl. Mater. Interfaces 2020, 12, 14599−14606

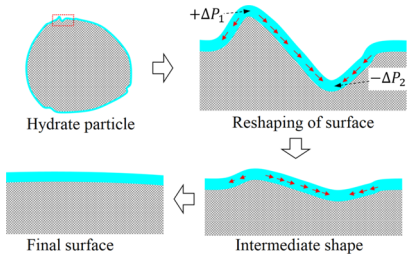

Figure 7. Conceptual illustration of the flattening of the hydrate surface due to the movement of quasi-liquid. Because of Laplace pressure, the pressure in the QLL is higher at the peak than at the valley. This pressure gradient drives a quasi-liquid flow, following the red arrows. Consequently, premelting is stimulated at the peak and new hydrate is formed at the valley, leading to the flattening of the hydrate surface. The drawings are not to scale.

form at the valley because of the arrival of quasi-liquid. This process flattens the hydrate surface and it only stops when a thermodynamically stable even surface of hydrate is attained (Figure 7).

The reshaping of hydrate particles as depicted in Figures 6 and 7 is thermodynamically favorable. However, the time scale of this process is not known yet and demands further investigations. In principle, the kinetics of reshaping would depend essentially on the temperature. The QLL becomes thinner and more viscous at larger degrees of subcooling and vice versa. Hence, the reshaping process would happen slowly at large subcooling but faster at low subcooling. In all cases, hydrate surfaces have a tendency to become smooth at infinite time scales.

It is instructive to consider two extremes. The first one is under extreme subcooling. In this case, the QLL vanishes and the hydrate particle behaves like a typical solid for that reshaping cannot occur. The second extreme situation is under extremely low subcooling ($\Delta T \rightarrow 0$), whereby the thickness of the QLL becomes infinite. The latter means that the whole hydrate particle is liquid-like and it behaves as a liquid droplet for that the reshaping process takes place instantly.

In Figure 8, we depicted a contact between a rough submillimeter hydrate particle and a substrate. Initially, the

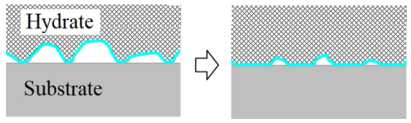

Figure 8. Conceptual illustration of the expansion of the contact area between a rough hydrate surface and a solid substrate. We ignore the roughness of the substrate for simplicity. The expansion of the contact area gives rise to the increasing adhesive force between the two surfaces, which is in agreement with the previous experiments. The drawings are not to scale.

total adhesion is sustained by a number of capillary bridges. The contact area grows as described above. The expansion of the contact area of each capillary bridge should lead to the increase in the total contact area. As such, one expects an increase in total adhesive force with increasing contact time. The proposed mechanism is confirmed by previous measurements by other groups based on a micromechanical force (MMF) apparatus.[12−15,35] In MMF experiments, a cyclopentane hydrate particle was placed at one end of a glass fiber (a cantilever) of the known spring constant. The hydrate particle was brought to attach to a substrate for a certain period (contact time) before it was forced to detach from the substrate. The force needed to separate the two objects was defined to be an adhesive force and it was deduced from the deflection of the cantilever in accordance with Hook's law. The measured adhesive force increased greatly with the increase in contact time.[12−15,35] This force normalized by the radius of the particle on a stainless-steel surface increased from ∼1 to ∼30 mN/m when the contact time prolonged from 1 s to 30 min.[12] Such an increase in the adhesive force indicates an expansion of the contact area between the hydrate particle and the substrate.

2.3. Hydrate Particle−Hydrate Layer Interactions. We have established a new model for the interactions between a hydrate particle and a pipe wall. These interactions dominate until a complete hydrate layer is formed on the pipe wall. Afterward, the interactions between hydrate particles and the pre-existing hydrate layer dominate. In principle, similar concepts can be used for interactions between hydrate particles and the hydrate layer. Equations 1−13 can be used. However, some parameters need to be changed accordingly. For example, A_{22} in eq 2 is identical with A_{11} because both surfaces are now hydrates. The parameter δ in all relevant equations has to be replaced by 2δ as there are now two QLLs involved. The contact angle θ is always zero. Thus, the capillary force between two hydrate surfaces is stronger than that between a hydrate particle and the pristine pipe wall.

2.4. Gravitational Force. Gravity may still affect the formation of hydrate plugs. The contribution of gravity to the adhesive forces between a hydrate particle and a pipe wall can be quantified by including gravitational force (F_g) in total adhesive force (F_{adh}).

$$F_{adh} = F_{ca} + F_g \tag{14}$$

$$F_g = -\frac{4}{3}\pi R^3 g \Delta\rho \times \cos\varphi \tag{15}$$

F_g has a negative sign because it acts as an adhesive force at the lower side of the pipe wall and as a detaching force at the upper side of the pipe wall. φ is the angle defined in Figure 3a, g is the gravitational acceleration, and $\Delta\rho = \rho_H - \rho_{oil}$ is the difference between density of gas hydrates ($\rho_H \cong 940$ kg/m^3, ref 8) and density of crude oils ($\rho_{oil} \cong 800$ kg/m^3, ref 36). Inserting typical numbers for the QLL shows that $4\pi R^3 g\Delta\rho/3$ only exceeds capillary forces for particles having radii in the order of 10^{-2} m. However, this would not be the case because hydrate particles in oil fluids typically have much smaller radii (discussed in Introduction). Therefore, capillary forces would always be a dominating force.

A possible effect of gravity is through an increased sedimentation of hydrate particles along the gravitational direction. Consequently, more hydrate particles arrive at the lower side than at the upper side of the pipe wall, which means that gravitational sedimentation increases the probability of hydrate particles to hit the bottom of the pipe and reduces the probability for hydrate particles to get into contact with the top wall. Such an influence of gravity leads to an increased thickness of the hydrate plug at the bottom side (Figure 2).

3. GENERAL DISCUSSION

3.1. Implications of Our Model. Our new model differs from the other available models by the following aspects: first, the origins of the capillary forces (or adhesive forces) are

https://dx.doi.org/10.1021/acsami.0c00636
ACS Appl. Mater. Interfaces 2020, 12, 14599−14606

different. Other models consider capillary bridges arising from water droplets. In hydrate suspensions having no water droplets, these models treat the hydrate particles to be "dry". Therefore, these models cannot describe the nanometer-range capillary forces that were observed by experiments. Our new model integrates the premelting behavior of hydrate surfaces into its concepts and successfully accounts for the nanometer-range capillary forces. Second, capillary bridges formed by the QLL can differ from those formed by water droplets. The differences might lie in variations in physicochemical parameters such as interfacial tension and contact angles between the ordinary liquid water and quasi-liquid water. Currently, it is not possible to compare these properties between ordinary water and quasi-liquid water because of lacking of experimental data. However, our model offers a pathway to make such assessments.

One may argue that the QLL becomes thinner and eventually disappears at sufficiently low temperature. Unfortunately, quantitative knowledge about the temperature-dependent thickness of the QLL on gas hydrate surfaces is still lacking. We found previously that the QLL on the surface of tetrabutyl ammonium bromide hydrate has a thickness of 11 nm at a subcooling of 13 °C. The QLL on the ice surface vanishes at a subcooling of around −30 °C.[30] One might assume an analogy between the structures of ice and gas hydrates and expect that the QLL on gas hydrates also disappears at a comparable subcooling. In such case, the hydrate surface would be dry and capillary force would vanish. However, a hydrate system at a subcooling of around −30 °C is likely unrealistic in industrial operations. Hence, the premelting of hydrate surfaces and the consequential capillary forces are likely inevitable in reality.

3.2. Prevention of Hydrate Plug Formation via Surface Coatings. Traditionally, chemicals are used to inhibit the formation of hydrate plugs.[37−44] The added chemicals such as methanol and ethylene glycol shift the equilibrium of hydrate formation to lower temperatures and/or higher pressures so that hydrates cannot form under the prevailing conditions. However, intensive use of chemicals raises concerns about the costs of production and negative impacts on the environment.[39−41] Alternatively, hydrophobic coating of the pipe wall is emerging as a promising chemical-free technique for preventing hydrate plug formation.[32−34] We have indicated that capillary forces, which act as attaching forces, between a hydrate particle and a pipe wall, decrease substantially when the contact angle θ of water on the pipe surface is increased (Figure 5b). Therefore, the use of super liquid-repellent surfaces can be an innovative method for the hydrate-plug prevention strategy. These surfaces are fabricated by grafting micro-hydrophobic pillars on a surface. Such structured surfaces have been shown to have excellent antiwetting behaviors.[45,46]

4. CONCLUSIONS

We have developed a new model of the interfacial interactions between a hydrate particle and a solid surface and between a hydrate particle and a hydrate surface. This model, for the first time, accounts for the premelting behavior of hydrate surfaces. Based on Laplace pressure, we proposed concepts of quasi-liquid flow in the premelting layer and the expansion of the contact area between a hydrate particle and a substrate. These concepts unravel the reshaping process of hydrate particles attaching to a solid surface or to a hydrate surface, which, in turn, leads to the consolidation of the hydrate. We quantified the contributions of vdW force, premelting-induced capillary force and gravitational force to the adhesive force between a hydrate particle and a solid surface (pipe wall). We showed that the adhesive forces between the hydrate particles and the pipe wall increase strongly when the surface of the pipe is more hydrophilic. We revealed an essential role of premelting-induced capillary force for the hydrate interactions. Our theoretical results agree well with the published experimental results. The findings are helpful for developing new methods for prevention of hydrate plug formation based on coating of pipe surfaces.

■ ASSOCIATED CONTENT

Supporting Information

The Supporting Information is available free of charge at https://pubs.acs.org/doi/10.1021/acsami.0c00636.

Formulation of eqs 5−12 based on the constant-volume method (PDF)

■ AUTHOR INFORMATION

Corresponding Authors

Ngoc N. Nguyen − *Physics at Interfaces, Max Planck Institute for Polymer Research, Mainz 55128, Germany; School of Chemical Engineering, Hanoi University of Science and Technology, Hanoi 100000, Vietnam;* orcid.org/0000-0002-0999-1176; Email: nguyenn@mpip-mainz.mpg.de

Hans-Jürgen Butt − *Physics at Interfaces, Max Planck Institute for Polymer Research, Mainz 55128, Germany; Earth-Life Science Institute, Tokyo Institute of Technology, Tokyo 152-8550, Japan;* orcid.org/0000-0001-5391-2618; Email: butt@mpip-mainz.mpg.de

Author

Rüdiger Berger − *Physics at Interfaces, Max Planck Institute for Polymer Research, Mainz 55128, Germany;* orcid.org/0000-0002-4084-0675

Complete contact information is available at: https://pubs.acs.org/10.1021/acsami.0c00636

Notes

The authors declare no competing financial interest.

■ ACKNOWLEDGMENTS

N.N.N. gratefully acknowledges the Alexander von Humboldt (AvH) Foundation for his AvH Fellowship for Postdoctoral Researchers (fellowship number: VNM 1200537 HFST-P).

■ REFERENCES

(1) Devold, H. *Oil and Gas Production Handbook: An Introduction to Oil and Gas Production, Transport, Refining and Petrochemical Industry*; ABB Oil and Gas: Aslo, 2013.

(2) Greaves, D.; Boxall, J.; Mulligan, J.; Montesi, A.; Creek, J.; Dendy Sloan, E.; Koh, C. A. Measuring the Particle Size of a Known Distribution Using the Focused Beam Reflectance Measurement Technique. *Chem. Eng. Sci.* **2008**, *63*, 5410−5419.

(3) Hammerschmidt, E. G. Formation of Gas Hydrates in Natural Gas Transmission Lines. *Ind. Eng. Chem.* **1934**, *26*, 851−855.

(4) Koh, C. A.; Sloan, E. D.; Sum, A. K.; Wu, D. T. In *Annual Review of Chemical and Biomolecular Engineering* Annual Reviews; Prausnitz, J. M., Ed.; Palo Alto, 2011; Vol. 2, pp 237−257.

(5) Bohrmann, G.; Torres, M. E. In *Marine Geochemistry*; Schulz, H. D., Zabel, M., Eds.; Springer Berlin Heidelberg: Berlin, Heidelberg, 2006; pp 481−512.

(6) Aman, Z. M.; Koh, C. A. Interfacial Phenomena in Gas Hydrate Systems. *Chem. Soc. Rev.* **2016**, *45*, 1678−1690.
(7) Sloan, E. D. Fundamental Principles and Applications of Natural Gas Hydrates. *Nature* **2003**, *426*, 353−359.
(8) Sloan, E. D.; Koh, C. A. *Clathrate Hydrates of Natural Gases*, 3rd ed.; CRC Press-Taylor & Francis Group: Boca Raton, 2008; Vol. *119*.
(9) Giavarini, C.; Hester, K. *Gas Hydrates: Immense Energy Potential and Environmental Challenges*; Springer London: London, 2011.
(10) Nguyen, N. N.; Nguyen, A. V. Hydrophobic Effect on Gas Hydrate Formation in the Presence of Additives. *Energy Fuels* **2017**, *31*, 10311−10323.
(11) Nguyen, N. N.; Nguyen, A. V.; Steel, K. M.; Dang, L. X.; Galib, M. Interfacial Gas Enrichment at Hydrophobic Surfaces and the Origin of Promotion of Gas Hydrate Formation by Hydrophobic Solid Particles. *J. Phys. Chem. C* **2017**, *121*, 3830−3840.
(12) Aman, Z. M.; Brown, E. P.; Sloan, E. D.; Sum, A. K.; Koh, C. A. Interfacial Mechanisms Governing Cyclopentane Clathrate Hydrate Adhesion/Cohesion. *Phys. Chem. Chem. Phys.* **2011**, *13*, 19796−19806.
(13) Aman, Z. M.; Leith, W. J.; Grasso, G. A.; Sloan, E. D.; Sum, A. K.; Koh, C. A. Adhesion Force between Cyclopentane Hydrate and Mineral Surfaces. *Langmuir* **2013**, *29*, 15551−15557.
(14) Hu, S.; Koh, C. A. Interfacial Properties and Mechanisms Dominating Gas Hydrate Cohesion and Adhesion in Liquid and Vapor Hydrocarbon Phases. *Langmuir* **2017**, *33*, 11299−11309.
(15) Liu, C.; Li, M.; Liu, C.; Geng, K.; Li, Y. Micromechanical Interactions between Clathrate Hydrate Particles and Water Droplets: Experiment and Modeling. *Energy Fuels* **2016**, *30*, 6240−6248.
(16) Aman, Z. M.; Sloan, E. D.; Sum, A. K.; Koh, C. A. Adhesion Force Interactions between Cyclopentane Hydrate and Physically and Chemically Modified Surfaces. *Phys. Chem. Chem. Phys.* **2014**, *16*, 25121−25128.
(17) Frostman, L. M.; Przybylinski, J. L. Successful Applications of Anti-agglomerant Hydrate Inhibitors. *SPE International Symposium on Oilfield Chemistry*; Society of Petroleum Engineers: Houston, Texas, 2001; p 10.
(18) Straume, E. O.; Morales, R. E. M.; Sum, A. K. Perspectives on Gas Hydrates Cold Flow Technology. *Energy Fuels* **2019**, *33*, 1−15.
(19) Nguyen, N. N.; Berger, R.; Butt, H.-J. Surface Premelting and Interfacial Interactions of Semi-Clathrate Hydrate. *J. Phys. Chem. C* **2019**, *123*, 24080−24086.
(20) Maeda, N. Is the Surface of Gas Hydrates Dry? *Energies* **2015**, *8*, 5361.
(21) Ally, J.; Vittorias, E.; Amirfazli, A.; Kappl, M.; Bonaccurso, E.; McNamee, C. E.; Butt, H.-J. Interaction of a Microsphere with a Solid-Supported Liquid Film. *Langmuir* **2010**, *26*, 11797−11803.
(22) Schellenberger, F.; Papadopoulos, P.; Kappl, M.; Weber, S. A. L.; Vollmer, D.; Butt, H.-J. Detaching Microparticles from a Liquid Surface. *Phys. Rev. Lett.* **2018**, *121*, 048002.
(23) Döppenschmidt, A.; Butt, H.-J. Measuring the Thickness of the Liquid-like Layer on Ice Surfaces with Atomic Force Microscopy. *Langmuir* **2000**, *16*, 6709−6714.
(24) Israelachvili, J. N. In *Intermolecular and Surface Forces*, 3rd ed.; Israelachvili, J. N., Ed.; Academic Press: San Diego, 2011; pp 253−289.
(25) Butt, H.-J.; Kappl, M. *Surface and Interfacial Forces*; Wiley-VCH Verlag GmbH & Co.: Weinheim, 2010.
(26) Haukalid, K.; Folgerø, K. Broad-Band Permittivity Measurements of Formation of Gas Hydrate Layers Using Open-Ended Coaxial Probes. *Energy Fuels* **2016**, *30*, 7196−7205.
(27) Bylov, M.; Rasmussen, P. Experimental Determination of Refractive Index of Gas Hydrates. *Chem. Eng. Sci.* **1997**, *52*, 3295−3301.
(28) Butt, H.-J. Capillary Forces: Influence of Roughness and Heterogeneity. *Langmuir* **2008**, *24*, 4715−4721.
(29) Butt, H.-J.; Kappl, M. Normal Capillary Forces. *Adv. Colloid Interface Sci.* **2009**, *146*, 48−60.
(30) Slater, B.; Michaelides, A. Surface Premelting of Water Ice. *Nat. Rev. Chem.* **2019**, *3*, 172−188.
(31) Li, Y.; Somorjai, G. A. Surface Premelting of Ice. *J. Phys. Chem. C* **2007**, *111*, 9631−9637.
(32) Das, A.; Farnham, T. A.; Bengaluru Subramanyam, S.; Varanasi, K. K. Designing Ultra-Low Hydrate Adhesion Surfaces by Interfacial Spreading of Water-Immiscible Barrier Films. *ACS Appl. Mater. Interfaces* **2017**, *9*, 21496−21502.
(33) Brown, E.; Hu, S.; Wang, S.; Wells, J.; Nakatsuka, M.; Veedu, V.; Koh, C. A. Low-Adhesion Coatings as a Novel Gas Hydrate Mitigation Strategy. *Offshore Technology Conference*; Offshore Technology Conference: Houston, Texas, 2017; Vol. *10*.
(34) Smith, J. D.; Meuler, A. J.; Bralower, H. L.; Venkatesan, R.; Subramanian, S.; Cohen, R. E.; McKinley, G. H.; Varanasi, K. K. Hydrate-Phobic Surfaces: Fundamental Studies in Clathrate Hydrate Adhesion Reduction. *Phys. Chem. Chem. Phys.* **2012**, *14*, 6013−6020.
(35) Aspenes, G.; Dieker, L. E.; Aman, Z. M.; Høiland, S.; Sum, A. K.; Koh, C. A.; Sloan, E. D. Adhesion Force between Cyclopentane Hydrates and Solid Surface Materials. *J. Colloid Interface Sci.* **2010**, *343*, 529−536.
(36) Schmidt, K. A. G.; Quiñones-Cisneros, S. E.; Kvamme, B. Density and Viscosity Behavior of a North Sea Crude Oil, Natural Gas Liquid, and Their Mixtures. *Energy Fuels* **2005**, *19*, 1303−1313.
(37) Sloan, E. D.; Subramanian, S.; Matthews, P. N.; Lederhos, J. P.; Khokhar, A. A. Quantifying Hydrate Formation and Kinetic Inhibition. *Ind. Eng. Chem. Res.* **1998**, *37*, 3124−3132.
(38) Nihous, G. C.; Kinoshita, C. K.; Masutani, S. M. A Determination of the Activity of Water in Water-Alcohol Mixtures Using Mobile Order Thermodynamics. *Chem. Eng. Sci.* **2009**, *64*, 2767−2771.
(39) Anderson, F. E.; Prausnitz, J. M. Inhibition of Gas Hydrates by Methanol. *AIChE J.* **1986**, *32*, 1321−1333.
(40) Kelland, M. A. History of the Development of Low Dosage Hydrate Inhibitors. *Energy Fuels* **2006**, *20*, 825−847.
(41) Mokhatab, S.; Wilkens, R. J.; Leontaritis, K. J. A Review of Strategies for Solving Gas-Hydrate Problems in Subsea Pipelines. *Energy Sources, Part A* **2007**, *29*, 39−45.
(42) Nguyen, N. N.; Nguyen, A. V. The Dual Effect of Sodium Halides on the Formation of Methane Gas Hydrate. *Fuel* **2015**, *156*, 87−95.
(43) Nguyen, N. N.; Nguyen, A. V.; Dang, L. X. The Inhibition of Methane Hydrate Formation by Water Alignment underneath Surface Adsorption of Surfactants. *Fuel* **2017**, *197*, 488−496.
(44) Nguyen, N. N.; Nguyen, A. V.; Nguyen, K. T.; Rintoul, L.; Dang, L. X. Unexpected Inhibition of CO2 Gas Hydrate Formation in Dilute TBAB Solutions and the Critical Role of Interfacial Water Structure. *Fuel* **2016**, *185*, 517−523.
(45) Butt, H.-J.; Vollmer, D.; Papadopoulos, P. Super Liquid-Repellent Layers: The Smaller the Better. *Adv. Colloid Interface Sci.* **2015**, *222*, 104−109.
(46) Butt, H.-J.; Roisman, I. V.; Brinkmann, M.; Papadopoulos, P.; Vollmer, D.; Semprebon, C. Characterization of Super Liquid-Repellent Surfaces. *Curr. Opin. Colloid Interface Sci.* **2014**, *19*, 343−354.

https://dx.doi.org/10.1021/acsami.0c00636
ACS Appl. Mater. Interfaces 2020, 12, 14599−14606